ACS APPLIED MATERIALS & INTERFACES

Research Article

www.acsami.org

Multifunctional 1D Magnetic and Fluorescent Nanoparticle Chains for Enhanced MRI, fluorescent Cell Imaging, And Combined Photothermal/Chemotherapy

Hui Wang,[†] Anton Mararenko,[†] Guixin Cao,[‡] Zheng Gai,[‡] Kunlun Hong,[‡] Probal Banerjee,[†] and Shuiqin Zhou*,[†]

[†]Department of Chemistry of The College of Staten Island and The Graduate Center, The City University of New York, Staten Island, New York 10314, United States

[‡]Center for Nanophase Materials Sciences, Oak Ridge National Laboratory, Oak Ridge, Tennessee 37831, United States

Supporting Information

ABSTRACT: While the assembled 1D magnetic nanoparticle (NP) chains have demonstrated synergistic magnetic effects from the individual NPs, it is essential to prepare new 1D NP chains that can combine the magnetism with other important material properties for multifunctional applications. This paper reports the fabrication and multifunctional investigation of a new type of 1D NP chains that combine the magnetic properties with fluorescent properties, photothermal conversion ability, and drug carrier function. The building block NPs are composed of magnetic Fe_3O_4 nanocrystals clustered in the core and fluorescent carbon dots embedded in the mesoporous carbon shell with hydroxyl/carboxyl groups anchored on their surface. These NPs can assemble under the induction of external magnetic field and form stable 1D NP chains of diameter ~90 nm and length ~3 μm via the hydrogen bonding and $\pi-\pi$ stacking linkage of the carbon shell. The resulted 1D hybrid NP chains not only demonstrate much higher magnetic resonance imaging (MRI) contrasting ability than the dispersed building block NPs, but also enter into intracellular region and light up the B16F10 cells under a laser excitation with strong and stable fluorescence. While the mesoporous carbon shell provides high drug loading capacity, the embedded fluorescent carbon dots convert near-infrared (NIR) light to heat, and hence kill the tumor cells efficiently and enhance the drug release rate to further improve the therapeutic efficacy under NIR irradiation. Such designed 1D magnetic-fluorescent hybrid NP chains with enhanced MRI contrast, fluorescent imaging ability, and combined chemo-/photothermal therapeutic ability have great potential for various biomedical applications.

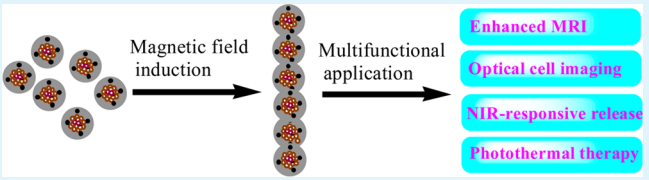

KEYWORDS: *1D nanochains, multifunction, enhanced MRI, drug carrier, photothermal therapy*

1. INTRODUCTION

Ordered one-dimensional (1D) nanostructures with a high aspect ratio have demonstrated exciting potential as imaging and sensing probes, drug and gene delivery carriers, and therapeutic agents.[1−9] Among the wide variety of nanomaterials, magnetic 1D nanostructures have received considerable attention because of their importance in cell manipulation, drug delivery, magnetic resonance imaging (MRI), microfluidics, and micromechanics.[10−19] For example, the ferromagnetic 1D nickel nanowires outperformed the corresponding magnetic nanoparticles (NPs) of comparable volume in cell separation.[11] The ferromagnetic nanowires in conjunction with patterned micromagnet arrays could control the spatial organization of mammalian cells.[13] However, these ferromagnetic 1D nanostructures carry a permanent magnetic moment and are thus susceptible to aggregate and precipitate in solution due to the magnetic dipolar attraction.[19,20]

The assembly of magnetic NPs into 1D ordered nanostructure is an alternative way to solve the aggregation puzzle. Different methods have been developed to fabricate the 1D iron oxide NP chains.[21−43] In general, the surface functionalized iron oxide NPs could be assembled through the specially designed molecular linkers, or electrostatic attractions, or anchored on solid substrates, or embedded on polymer chain templates such as DNA, protein fibril, and other polyelectrolytes. The assembly of these magnetic NPs can be directed along the 1D direction under the guidance of external magnetic field. The assembled interparticle distance and chain length can be controlled through the selection of surface capping agents on the iron oxide NPs and template matrix. The 1D magnetic NP chains prepared through the assembly of the iron oxide NPs demonstrate excellent synergistic effects from the individual NPs, which not only maintain the superparamagnetic behavior, but also enhance the saturation magnetization and other magnetic functions. For instance, the 1D magnetic NP chains can enter living cells for cell manipulation and microrheology.[29] These NP chains can significantly enhance the MRI contrast compared to the dispersed iron oxide

Received: June 16, 2014
Accepted: August 15, 2014
Published: August 15, 2014

NPs.[31−34] They also exhibit superior magnetic hyperthermia response for potential cancer therapy in comparison with the randomly distributed iron oxide NPs.[41] Although these improved magnetic properties of the 1D NP chains are exciting, the applications of the 1D NP chains based on magnetic function alone are still limited. To meet the desirable multifunctional needs in biomedical applications, it is essential to combine the magnetism with other important material properties into the 1D NP chains. So far, few studies have been reported on multifunctional 1D iron oxide NP chains. Berret's group fabricated 1D nanorods through the coassembly of negatively charged organic fluorescent colloids and poly(acrylic acid) capped iron oxide NPs in the presence of cationic polyelectrolyte as linkers.[27] The resulting 1D nanorods exhibit both magnetic and emissive properties, and thus can potentially be used for MRI and fluorescent bimodal imaging contrast agent. Karathanasis' group fabricated multicomponent nanochains through the assembly of magnetic iron oxide NPs with the drug-loaded liposome.[39,40] The magnetic iron oxide NP chains could serve as a mechanical transducer to transfer the radio frequency energy to the drug-loaded liposome, which caused defects on the liposomal walls and thus triggered the drug release capable of spreading throughout the entire tumor. The surface functionalization with a targeting ligand of the NP chains could further enhance the treatment efficacy of difficult-to-reach cancer sites such as the micrometastasis sites.

In the present work, we report a new method to prepare the multifunctional 1D magnetic NP chains to combine the enhanced MRI contrast, fluorescent imaging ability, and photothermal/chemotherapy into a single 1D nano-object. Our strategy involves the first one-pot solvothermal synthesis of multifunctional magnetic iron oxide-carbon composite NPs, followed by the induction of external magnetic field to form 1D NP chains. While the magnetic field-induced 1D assembly of carbon coated iron oxide NPs has been previously reported,[42,43] no attention has been paid to prepare the fluorescent carbon shell and the multifunctional properties of the magnetic 1D NP chains for biomedical applications have not been explored. Herein, we redesign and synthesize new building blocks of iron oxide-fluorescent carbon (Fe_3O_4@FC) composite NPs with fluorescent carbon dots embedded in the porous carbon shell and discrete Fe_3O_4 nanocrystals clustered in the core (see Figure 1a). In such a design, the porous and fluorescent carbon shell not only serves as drug carriers with high drug loading capacity, but also as optically active component for fluorescent cellular imaging and NIR photothermal conversion. The magnetic field-induced assembly of these Fe_3O_4@FC composite NPs result in highly persistent 1D nanochains with a diameter of 90 nm and a length about 0.3−3 μm, depending on the assembly time of building block NPs. The magnetic 1D NP chains were surrounded by the fluorescent carbon shell and thus manifest both weakly ferromagnetic and strong photoluminescent (PL) properties. Because of the weakly ferromagnetic property and the hydrophilic surface functional groups (hydroxyl and carboxyl) on the porous carbon shell, the as-synthesized 1D Fe_3O_4@FC NP chains do not carry a permanent magnetic moment and have no spontaneous aggregation in aqueous dispersion, which allows us to explore their multifunctional applications in biomedical field. In addition to the significant enhancement of the MRI contrast, we show that the 1D Fe_3O_4@FC NP chains can enter into the intracellular region and light up the mouse melanoma cells B16F10 under laser excitation. Furthermore, benefited from the efficient photothermal conversion ability of the carbon dots embedded in the carbon shell, an exogenous NIR irradiation can significantly kill the B16F10 cells. Thus, the 1D Fe_3O_4@FC NP chains can combine the chemotherapy with NIR photothermal treatment to further enhance the therapeutic efficacy.

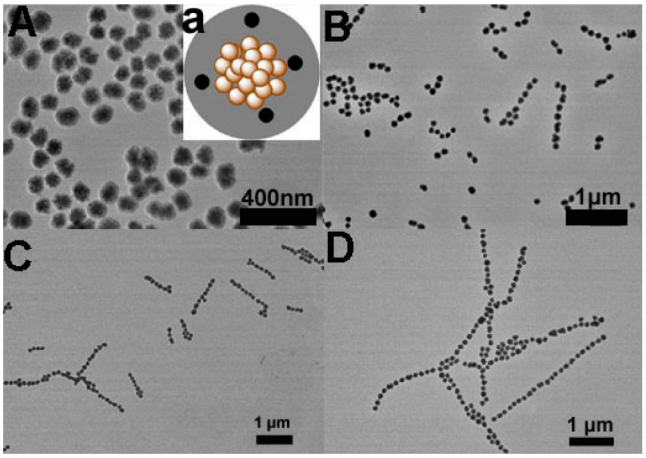

Figure 1. TEM images of the Fe_3O_4@FC NPs and their assembled 1D NP chains formed at different magnetization time. (A) 0, (B) 1, (C) 3, and (D) 12 h. The inset a in A is a schematic diagram for the nanostructure of a single Fe_3O_4@FC NP.

2. EXPERIMENTAL SECTION

2.1. Materials. All chemicals were purchased from Aldrich. Ferrocene ($Fe(C_5H_5)_2$, ≥98%), hydrogen peroxide (H_2O_2, 30%), acetone (C_3H_6O) and ethanol (C_2H_6O) were used as received without further purification. The water used in all experiments was of Millipore Milli-Q grade.

2.2. Synthesis of Fe_3O_4@FC Building Block NPs. The Fe_3O_4@FC NPs were synthesized via a one-step solvothermal method.[44] Ferrocene (0.10 g) were dissolved in 30 mL of acetone in a 100 mL beaker covered with a foil to avoid the volatilization of acetone. After intense sonication for 30 min, 2.5 mL of 30% H_2O_2 solution was added dropwise by hand using a pipette within 1 min while stirring. The resulted mixture solution was then vigorously stirred for 30 min with a magnetic stirring apparatus under ambient conditions. Afterward, the precursor solution was transferred to the Teflon-lined stainless autoclave with the total volume of 50.0 mL, and then heated to and maintained at 200 °C. After 48 h, the autoclave was cooled naturally to room temperature. The products from the autoclave were washed with ethanol three times to remove excess ferrocene and collected for further experiments.

2.3. Synthesis of 1D Fe_3O_4@FC NP Chains. The formation of 1D Fe_3O_4@FC NP chains resulted from the assembly of the Fe_3O_4@FC NPs under the induction of an external magnetic field. First, the as-synthesized Fe_3O_4@FC NPs were dispersed into ethanol solvent and formed a homogeneous suspension with a concentration of 2.0 mg/mL. After intense sonication for 30 min, the suspension was magnetized for certain period of time by a 0.30 T rare earth neodymium magnet (model N52, 2 cm × 2 cm × 1 cm) to allow the slow assembly of NPs. The magnet's north and south poles are on the opposite 2 cm × 2 cm faces. To study the influence of the magnetization time on the length of the resulting 1D Fe_3O_4@FC NP chains, different magnetization time of 0, 1, 3, and 12 h have been compared. Finally, the 1D Fe_3O_4@FC NP chains attracted on the bottom of container were collected and washed with ethanol three times and dried at room temperature in a vacuum oven.

2.4. Internalization of 1D Fe_3O_4@FC NP Chains into Mouse Melanoma Cells B16F10. Round glass coverslips were placed in wells of a 24-well plate and treated with 0.1% poly-L-lysine in 100 mM phosphate buffered saline (PBS) for 40 min. Following the treatment, the solution was aspirated and the wells were washed with PBS 3 times

each. Next, B16F10 cells (2×10^4cell/well) were plated on the glass coverslips at 80% confluence in DMEM containing 10% FBS and 1% penicillin-streptomycin. After 24 h, 500 μL of Fe_3O_4@FC NP chains of 50 mg/mL in serum-free DMEM were respectively added to the marked wells. In a control well, 500 μL of serum-free DMEM was added. The plate was incubated at 37 °C for 2 h. The medium was then aspirated and fresh serum-free DMEM was added to each well. Finally, the coverslips attached with cells were removed from the wells and mounted onto slides for confocal microscopy study.

2.5. Drug Loading and Release of the 1D Fe_3O_4@FC NP Chains. The drug loading were performed by adding 1 mg of 1D Fe_3O_4@FC NP chains into 10 mL of PBS solution (0.005 M, pH 7.4) containing 1 mg of doxorubicin (DOX) drug under magnetic stirring at 37 °C for 48 h. Then the DOX-loaded 1D Fe_3O_4@FC NP chains were separated by a 0.20 T magnet. To remove the unloaded DOX absorbed on the surface, we washed the precipitate and redispersed it in 10 mL of PBS solution of pH 7.4. The procedure of magnetic separation, washing, and redispersion was repeated for five times. All the supernatants and washed solutions were combined and used for the UV−vis spectrophotometric analysis of unloaded DOX at 480 nm. The drug loading content of the 1D NP chains were calculated by $(M_0 - M_u)/M_n \times 100\%$, where M_0 and M_u are the mass of DOX in the initial solution and the separated solution, respectively. M_n is the mass of the 1D Fe_3O_4@FC NP chains used in the loading process. The in vitro release of DOX from the 1D NP chains was evaluated by the dialysis method. The purified DOX-loaded NP chains were redispersed in 10 mL of PBS solution (0.005 M, pH 7.4). Two dialysis bags filled with 5 mL of suspension of DOX-loaded 1D Fe_3O_4@FC NP chains were respectively immersed in 50 mL PBS buffer (0.005 M, pH 7.4) at 37 °C without or with NIR light at an output power of 1.5 W/cm^2. The released DOX outside of the dialysis bag was sampled at certain interval and assayed by UV−vis spectrometry at 480 nm.

2.6. In Vitro Cytotoxicity of DOX-Free and DOX-Loaded 1D Fe_3O_4@FC NP Chains with or without NIR Irradiation. B16F10 cells were cultured in 96-well microplate with 100 μL of medium containing about 2000 cells seeded into each well. After an overnight incubation for attachment, the medium was removed. Another 100 μL medium containing the DOX-free and DOX-loaded 1D Fe_3O_4@FC NP chains at different final concentrations of 200, 150, 100, and 50 μg/mL was, respectively, added into each well. Wells used the normal medium without drugs were used as control. For photothermal treatments, the cells were irradiated with 1.5 W/cm^2 NIR light for 5 min. After being incubated for 24 h, 10 μL of 3-(4,5-dimethyl-2-thiazolyl)-2,5-diphenyltetrazolium bromide (MTT) solution (5 mg/mL in PBS) was added into the wells. The cells were continuously incubated in a humidified environment of 5% CO_2 and 37 °C for 2 h. The medium was then removed and 100 μL of DMSO was added to each well. The plates were gently agitated until the MTT formazan precipitate dissolved. Cell viability was measured using a microplate reader at 570 nm.

2.7. Characterization. Field emission scanning electron microscopy (FE-SEM) images were performed on AMRAY 1910 scanning electron microscope. Transmission electron microscopy (TEM) images were taken on an FEI TECNAI transmission electron microscope at an accelerating voltage of 120 kV. High-resolution TEM (HRTEM) images were taken on JEM 2100 (JEOL) microscope with an acceleration voltage of 200 kV. Energy-dispersive X-ray (EDX) analysis was obtained with an EDAX detector installed on the same HRTEM. The FT-IR spectrum of the product sample was recorded with a Nicolet Instrument Co. MAGNA-IR 750 Fourier transform infrared spectrometer.The UV−vis absorption spectra were obtained on a Thermo Electron Co. Helios β UV−vis Spectrometer. The PL spectra were obtained on a JOBIN YVON Co. FluoroMax-3 Spectrofluorometer equipped with a Hamamatsu R928P photomultiplier tube, calibrated photodiode for excitation reference correction from 200 to 980 nm, and an integration time of 1 s. The B16F10 cells incorporated with the 1D Fe_3O_4@FC NP chains were imaged using a confocal laser scanning microscopy (LEICA TCS SP2 AOBS) equipped with a HC PL APO CS 20 × 0.7 DRY len and three lasers of different wavelengths (405, 488, and 546 nm). A superconducting quantum interference device (SQUID) magnetometer (Quantum Design MPMS XL-7) was used to measure the magnetic properties of the 1D Fe_3O_4@FC NP chains. Relaxation properties of the dispersed Fe_3O_4@FC NPs and their assembled 1D NP chains in aqueous solution were measured at 25 °C with small animal 7.0 T MR scanner (Varian, USA) with a 63/95 mm quad birdcage coil and gradient strength up to 400 mT/m.

3. RESULTS AND DISCUSSION

The strategy to prepare the 1D Fe_3O_4@FC NP chains involves the first preparation of the Fe_3O_4@FC NPs with magnetic Fe_3O_4 nanocrystals clustered in the core and fluorescent carbon dots embedded in the amorphous carbon shell, followed by the assembly of these NPs under the induction of an external magnetic field of 0.30 T. Figure 1 shows typical TEM images of the as-assembled 1D Fe_3O_4@FC NP chains formed at different magnetization time. Without applying external magnetic field, the Fe_3O_4@FC NPs are randomly dispersed in disordered arrangement (Figure 1A). The FT-IR spectrum of the Fe_3O_4@FC NPs (see the Supporting Information, Figure S1a) demonstrates strong absorption peaks at 1555 and 1402 cm^{-1}, which can be attributed to the C═C stretching vibration and the skeletal/ring C−C stretching modes of polyaromatic systems in the carbon shell, respectively.[44−47] The peak at 1667 cm^{-1} should be from the carbonyl stretching conjugated with the condensed aromatic carbons.[47] The weak shoulder at ∼1702 cm^{-1} can be assigned to the carbonyl stretching in carboxylic acid (−COOH) groups and the broad peak at about 3423 cm^{-1} can be attributed to the −OH stretching modes.[46,47] The hydrophilic surface −OH and −COOH groups explain the excellent dispersibility of the Fe_3O_4@FC NPs in water and other polar solvents. After the introduction of external magnetic field, the transition of nanostructure from zero dimensional (0D) NPs to 1D nanochains is obviously observed, which indicates that the 1D magnetic NP chains was successfully synthesized using the magnetic induction. The length of the 1D NP chains depends on the magnetization time (Figure 1B−D). The quantitative length distributions of the NP chains as a function of magnetic assembling time are displayed in Figure S2 in the Supporting Information, which clearly demonstrates that the chain length increases with the magnetization time until the assembling process is completed. When the magnetization time increases to 12 h, nearly no individual NPs exist and long 1D NP chains of an average length about 3 μm are obtained. Further increase in the magnetization time has no significant effect on the length of the 1D NP chains, indicating that the magnetic field-induced assembly of the NPs completed within 12 h. Figure S3 in the Supporting Information shows a schematic illustration for the formation of the 1D Fe_3O_4@FC NP chains under magnetic induction. After an external magnetic field was introduced under the bottom of the suspension of colloidal NPs (stage I), these NPs tend to get closer and reorient along the lines of magnetic force in a head-to-tail configuration to form a nanochain structure (stage II, confirmed in Figure 1B). The reason is that the anisotropic field-induced magnetic dipolar interaction of these NPs is stronger than the Brownian motion and electrostatic repulsion. With an increase in the magnetization time, the short NP chains will further grow up to form long chains along the direction of magnetic force (stage III). Because the carbon shell of the Fe_3O_4@FC NPs carries −OH and −COOH groups, the carbon shell of the adjacent magnetically driven closely attached

NPs further integrate by the hydrogen bonds among these surface functional groups, leading to the formation of carbon shell-linked 1D NP chains (stage IV). Compared to the FT-IR spectrum of the dispersed NPs, the absorption peaks at 3423 cm^{-1} for −OH groups and C═O groups in −COOH at 1702 cm^{-1} respectively shifted to 3507 and 1709 cm^{-1} in the assembled 1D NP chains (see Figure S1b in the Supporting Information), respectively, which suggests the hydrogen bonding interactions of these groups between the adjacent NPs enhanced because of the alignment. In addition, the peaks at 1555 cm^{-1} for the C═C vibration and at 1402 cm^{-1} for the skeletal/ring C−C stretching modes of polyaromatic systems in the carbon shell of NPs also shifted to 1562 and 1415 cm^{-1} respectively in the assembled 1D NP chains, which may indicate possible stronger $\pi-\pi$ stacking interactions between the carbon shells of adjacent NPs. The linkage between the carbon shell of adjacent NPs through hydrogen bonds and $\pi-\pi$ stacking enables the assembled 1D NP chains to remain chain structure stable even after the removal of external magnetic field. Importantly, the resulted 1D Fe_3O_4@FC NP chains can still be easily dispersed into water with no obvious further aggregation (see Figure S4a in the Supporting Information), which is necessary for bioapplications such as cell guidance and cell separation. Interestingly, these randomly dispersed 1D NP chains can further align in order along the direction of magnetic force (see Figure S4b in the Supporting Information), indicating that an external magnetic field can easily manipulate the behavior of these 1D NP chains. It should be mentioned that our synthetic conditions for the Fe_3O_4@FC NPs may also generate a wide variety of organic molecules including fluorescent molecules. However, these fluorescent organic molecules are soluble in ethanol but without magnetic property. In our approach, the synthesized Fe_3O_4@FC building block NPs were magnetically separated, washed with ethanol, and redispersed in ethanol for assembling into the 1D NP chains under the magnetic induction. The magnetically collected 1D NP chains were finally washed with ethanol three times again before drying. In such a procedure, the fluorescent organic molecules can be removed from the solid product of 1D Fe_3O_4@FC NP chains because these organic molecules cannot be magnetically separated and remained in the ethanol solution phase.

The SEM image of the 1D Fe_3O_4@FC NP chains in Figure 2A further confirms that the NP chains are in standard linear structure and well-dispersed in water because of their hydrophilic surfaces. The TEM image of a single chain (Figure 2B) shows that the 1D Fe_3O_4@FC NP chain with a length of about 4 μm is composed of linked NPs with diameter about 90 nm. It is noteworthy that the sample of 1D Fe_3O_4@FC NP chains used for this TEM study was treated with ultrasonication in the absence of external magnetic field, which shows the excellent structured stability of the 1D NP chains. The inset in Figure 2B confirms that the high stability of the NP chains result from the linkage of the fluorescent carbon shell of the NPs, leading to the 1D NP chains coated by the carbon shell. The HRTEM image (Figure 2C) further reveals the existence of the overlapped organic carbon materials between adjacent NPs. Some small nanocrystals with size about 4 nm can be found in the overlapped carbon matrix (red circled). The EDX spectrum (Figure 2D) of the small-sized nanocrysyal only shows the existence of C and Cu elements, indicating that the small nanocrystal should be attributed to the fluorescent carbon dot (Cu from the copper grid). In addition, the clear 2D lattice

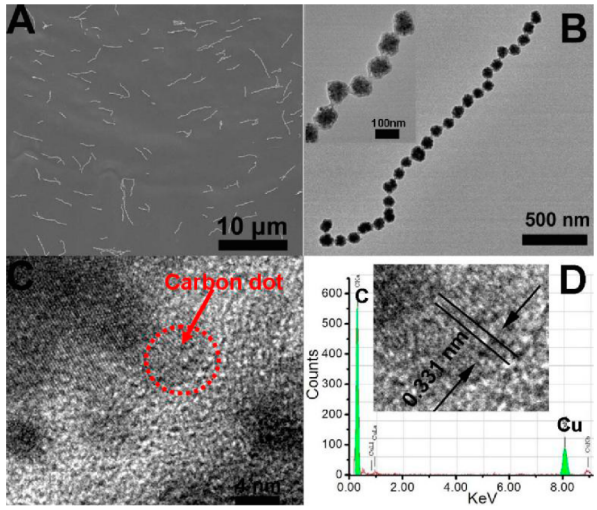

Figure 2. (A) SEM image of the 1D Fe_3O_4@FC NP chains; (B) TEM image and magnification of single 1D Fe_3O_4@FC NP chain; (C) HRTEM image of the organic carbon layer between adjacent NPs with carbon dots marked in red circle; (D) EDS and lattice fringe (inset) of the single carbon dot.

fringes (inset in Figure 2D) of the fluorescent carbon dot exhibit an interplanar distance of about 0.331 nm, which corresponds well to the (006) lattice planes of graphitic carbon.[48]

Figure 3A shows typical UV−vis absorption spectrum of the as-obtained 1D Fe_3O_4@FC NP chains. A sharp absorption at about 260 nm is clearly observed, which is likely originated from the formation of multiple polyaromatic chromophores and indicates the existence of fluorescent carbon dots.[49,50] In addition, a relatively weak and broad absorption band around 390 nm can be found. When the aqueous dispersion of the 1D Fe_3O_4@FC NP chains was exposed under a UV light of 365 nm, the blue light was emitted from the dispersion (inset b of Figure 3A). Figure 3B shows the evolution of the PL spectra of the 1D Fe_3O_4@FC NP chains under different excitation wavelength. When the excitation wavelength increases from 320 to 560 nm, the emission peak red-shifts to longer wavelength and the PL intensity gradually increases, which indicate a distribution of the different surface energy traps of the carbon dots embedded in the carbon shell.[51] More importantly, the Fe_3O_4@FC NP chains also exhibit upconverted PL property. Figure 3C demonstrate the PL spectra of the 1D Fe_3O_4@FC NP chains excited by long-wavelength light from 700 to 540 nm. The corresponding upconverted emissions locate in the range from 530 to 420 nm, which should be attributed to the multiphoton active process similar to previously reported carbon dots.[52] It should be noted that the 1D Fe_3O_4@FC NP chains exhibit excellent photostability. As shown in Figure S5 in the Supporting Information, the maximum PL intensity of the 1D NP chains in aqueous phase has negligible changes (8.2%) after 2 h continuous exposure to the excitation light of 496 nm in wavelength using a fluorescence spectrophotometer with the ozone-free xenon arc lamp (150 W) as light source. In contrast, the maximum PL intensity of Rhodamine B dye solution decreases by 31% under the same experimental conditions. The maximum PL intensity of fluorescein dye solution decreases by 31% after 2 h continuous exposure to an excitation light of 360 nm using the same fluorometer. These results indicate that our Fe_3O_4@FC NP chains possess much better photostability than

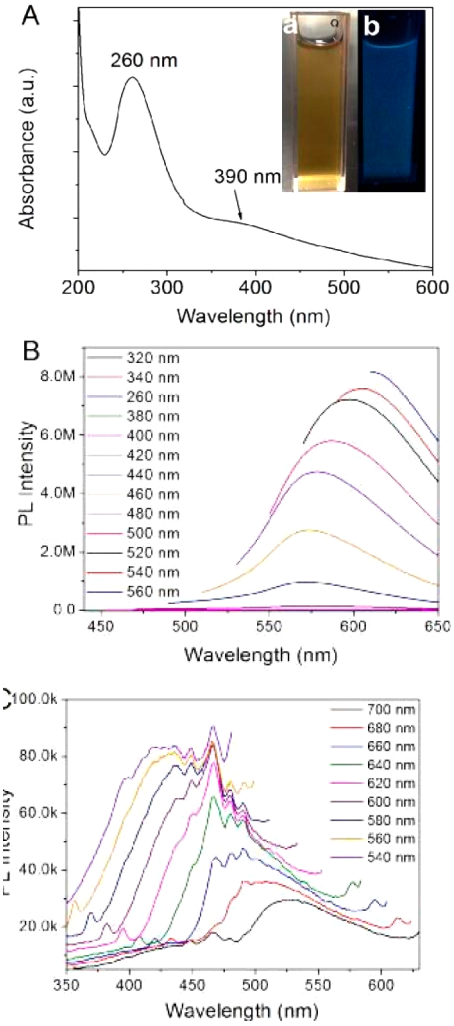

Figure 3. (A) UV−vis spectrum of the as-obtained 1D Fe_3O_4@FC NP chains dispersed in water. The inset is photographs of the aqueous dispersion of the NP chains under visible light (a) and UV light (b, 365 nm), respectively. (B) Fluorescence spectra and (C) Up-converted fluorescence spectra of the 1D Fe_3O_4@FC NP chains dispersed in water under different excitation wavelength.

organic dyes. The strong excitation wavelength-dependent and upconverted fluorescence with excellent photostability against light illumination and air exposure make the 1D Fe_3O_4@FC NP chains advantageous over organic dyes for biosensing and bioimaging applications.[53,54]

Figure 4A shows the magnetic hysteresis loop of the Fe_3O_4@FC NPs and their assembled 1D Fe_3O_4@FC NP chains measured at 300 K in an applied magnetic field of up to 40 000 Oe. An expanded plot in the inset for field strengths between −40 and 40 Oe reveals a weakly ferromagnetic nature of the NP chains at room temperature. The temperature dependence of zero-field-cooled (ZFC) and field-cooled (FC) magnetization for the 1D NP chains is presented in Figure 4B. The ZFC and FC curves separate from each other from 5 to 325 K and no transition from ferromagnetism to superparamagnetism can be observed, which further confirms the weak ferromagnetism of the 1D Fe_3O_4@FC NP chains at room temperature.[55] In addition, the 1D Fe_3O_4@FC NP chains exhibit a larger saturation magnetization (Ms) of 35.9 emu/g in comparison with that of the corresponding randomly dispersed Fe_3O_4@FC building block NPs (32.0 emu/g) due to the formation of 1D

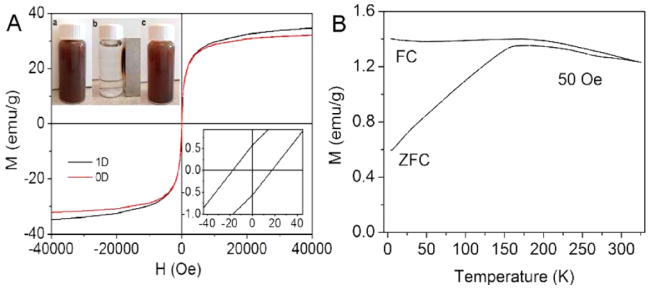

Figure 4. (A) Hysteresis loop measured at room temperature for the Fe_3O_4@FC NPs (0D) and their corresponding 1D Fe_3O_4@FC NP chains (1D). The left inset is photographs of the aqueous dispersions of the 1D Fe_3O_4@FC NP chains (a) without magnetic field; (b) with 0.30 T magnetic field for 1 min; and (c) after removal of the magnetic field. The right inset shows the respective expanded plots of the 1D NP chains for field between −40 and 40 Oe. (B) Zero-field-cooling (ZFC) and field-cooling (FC) curves of the as-obtained 1D Fe_3O_4@FC NP chains measured in an applied field of 50 Oe.

ordered nanostructure.[10] When the aqueous dispersion of the as-obtained 1D Fe_3O_4@FC NP chains is subjected to a magnetic field (0.30 T), the sample can be attracted toward the magnet side within minutes, as shown in inset b of Figure 4A. Slight agitation will bring the 1D Fe_3O_4@FC NP chains back into the original uniform dispersion in water after the magnetic field was removed (inset c in Figure 4A). The fast redispersing ability of the 1D Fe_3O_4@FC NP chains in water should be attributed to their weak ferromagnetism property and surface −COOH and/or −OH groups. The newly developed 1D Fe_3O_4@FC NP chains with quick magnetic response and exceptional colloidal stability in water have great advantage for bioapplications over those ferromagnetic electrodeposited 1D nanowires with a permanent magnetic moment and a strong tendency to aggregate.[19,20]

Considering the excellent magnetic properties and colloidal stability in aqueous phase, it is expected that the developed 1D Fe_3O_4@FC NP chains should have high MRI contrasting ability. Figure 5A shows the inverse relaxation times $1/T^*_2$ of the dispersed Fe_3O_4@FC NPs (0D) and the assembled 1D Fe_3O_4@FC NP chains at different concentrations. The specific relaxivity (r^*_2) of the 1D NP chains was calculated to be 960.9 mM^{-1} s^{-1} using a clinical 7.0 T MRI instrument, which reveals that the 1D Fe_3O_4@FC NP chains have higher potential as T^*_2 contrast agents for cancer diagnosis than the dispersed building block NPs (674.4 mM^{-1} s^{-1}). The increase in the transverse relaxivity resulting from the chaining of the Fe_3O_4@FC NPs NPs is in consistent with the result recently reported by Ivanisevic's group, in which the magnetic NP chains formed on DNA template possess much higher r_2 than their corresponding dispersed NPs.[33] It should be mentioned that this chaining effect of magnetic NPs on the r_2 increase is in opposite to the one observed in Saville et al.'s work, in which the chaining of polymer-coated magnetic NPs in the magnetic field leads to a time dependent decrease in r_2 as the NPs form chains.[56] This chaining-induced r_2 decrease in the polymer-coated magnetic NPs should be attributed to the ultralarge size of the linear aggregates with average chains length from about 5 to 30 μm, which has moved into the echo-limited regime. Figure 6B reveals that the MRI signal intensity declines with the increase in concentration of the 1D Fe_3O_4@FC NP chains and the dispersed Fe_3O_4@FC NPs (expressed in iron concentration), because the magnetic Fe_3O_4 nanocrystals shorten the T^*_2 by

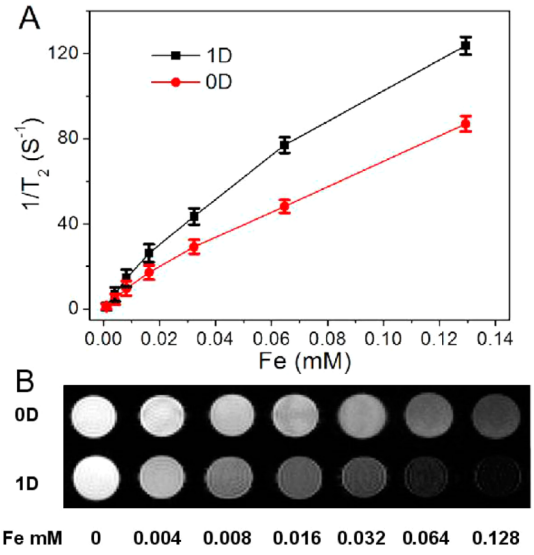

Figure 5. (A) T^*_2 relaxation rates and (B) T^*_2-weighted MR images as a function of iron concentration (mM) for the dispersed Fe_3O_4@FC NPs (0D) and their assembled linear Fe_3O_4@FC NP chains (1D), respectively.

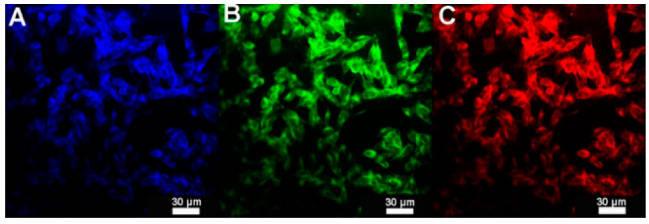

Figure 6. Scanning confocal microscopy images of B16F10 cells after incubated with the 1D Fe_3O_4@FC NP chains for 2 h under different excitation wavelength. (A) 405, (B) 488, and (C) 546 nm.

dephasing the spins of neighboring water protons.[57] The progressively enhanced darkness in the T^*_2-weighted MRI is obviously observed with the elevated Fe concentration from 0 to 0.128 mM. Compared to the dispersed Fe_3O_4@FC NPs at the same concentrations, the 1D structured Fe_3O_4@FC NP chains exhibit much darker T^*_2-weighted MRI signals. Such an enhancement in the T^*_2-weighted MRI contrasting ability of the 1D structured NP chains results from the increased magnetization and local magnetic field strength of the assembled Fe_3O_4@FC NP chains, which influence surrounding protons to transversely relax faster compared to the local magnetic fields produced by the dispersed Fe_3O_4@FC NPs. All these results show that the ordered 1D nanostructured NP chains have better MRI contrast than the dispersed NPs, which is consistent with the reported results.[33]

As demonstrated above, the 1D Fe_3O_4@FC NP chains possess stable, strong, and excitation wavelength-tunable PL properties. In addition to the excellent MRI contrasting ability, we expect that the 1D Fe_3O_4@FC NP chains should also have additional function for fluorescent cellular imaging label. Figure 6 shows the laser scanning confocal microscopy images of the mouse melanoma B16F10 cells after incubated with the 1D Fe_3O_4@FC NP chains for 2h. No signs of morphological damage to the cells were observed, suggesting a minimal cytotoxicity of the 1D NP chains. The 1D Fe_3O_4@FC NP chains demonstrate multicolor fluorescence imaging ability for the cells under different excitation wavelengths. This phenomenon may originate from the different sizes of the fluorescent carbon dots embedded in the carbon shell of the NP chains. The z-scanning confocal micrographs shown in Figure S6 in the Supporting Information reveal that the 1D Fe_3O_4@FC NP chains can be successfully internalized into the B16F10 cells without inducing cell death. Considering the similarity of the 1D structure of the Fe_3O_4@FC NP chains to that of carbon nanotube, the way of our 1D Fe_3O_4@FC NP chains entering into the cell should be similar to that of carbon nanotubes, either via classic endocytic pathways or by direct penetration through the lipid bilayer of cell membrane.[58−60] The excellent photostability of the 1D Fe_3O_4@FC NP chains was further confirmed in the laser scanning confocal images of the NP chains-incubated B16F10 cells under a continuous exposure to the excitation laser. As shown in Figure S7 in the Supporting Information, with prolonged irradiation time from 0 to 30 min under the 488 nm excitation laser, no obvious fluorescent signal changes could be observed in the cellular images. The results suggest that the as-obtained 1D Fe_3O_4@FC NP chains with excellent photostability can be used for long-term fluorescent cellular imaging. Furthermore, the upconversion PL property of the 1D Fe_3O_4@FC NP chains may be used for bioimaging under excitation of NIR light, which can penetrate into biological tissues more effectively than visible light. As demonstrated in Figure S8a in the Supporting Information, the glass coverslip attached with unlabeled B16F10 cells cannot be observed in the Odyssey CLx infrared imaging system with NIR excitation wavelength of λ_{ex} = 700 and 800 nm, because the unlabeled cells do not emit fluorescence. In contrast, the coverslip attached with the B16F10 cells incubated with our 1D NP chains can be clearly imaged under the excitation of same NIR light (see Figure S8b in the Supporting Information), benefited from the bright fluorescence emitted from the 1D NP chains internalized in the cells under the NIR light excitation.

After demonstrating the MRI and fluorescent imaging ability, we next investigate the function of the 1D Fe_3O_4@FC NP chains for NIR light-responsive drug carriers using DOX as a model drug. Due to the mesoporous structure of the carbon shell of the 1D NP chains and the strong interactions of the DOX molecules with the carboxyl and hydroxyl groups of the carbon shell,[61] the DOX molecules are readily loaded into the mesoporous carbon shell by simply mixing the 1D Fe_3O_4@FC NP chains in the PBS solution of DOX, which can be evidenced by the significant variation of UV−vis absorption peak of the 1D NP chains before and after loading the DOX drug (see Figure S9 in the Supporting Information). The drug loading content of DOX in the 1D Fe_3O_4@FC NP chains was determined to be 804 mg/g, which means that 1D Fe_3O_4@FC NP chains can be used as a promising drug carrier with high drug loading capacity. Figure 7 shows the in vitro releasing behavior of DOX drug from the 1D Fe_3O_4@FC NP chains in the PBS solution of pH 7.4 at 37 °C in the absence and presence of 1.5 W/cm^2 NIR light irradiation for 5 min at different releasing stages. Without NIR radiation, the release of DOX from the 1D Fe_3O_4@FC NP chains is slow but at a nearly steady rate of about 1.1%/h from fifth to 60th hour, which should be mainly controlled by the diffusion rate of the DOX molecules from the pores of carbon shell to exterior solution. It took about 95 h for 95% of the loaded DOX to be released. In contrast, the introduction of 5 min NIR radiation could dramatically enhance the DOX releasing rate. For example, right after the 5 min NIR irraditation at the fifth hour, the

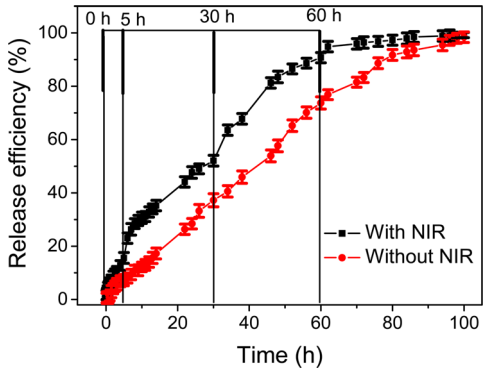

Figure 7. Releasing profiles of the DOX drug from the 1D Fe_3O_4@FC NP chains at 37 °C, irradiated with/without 1.5 W/cm^2 NIR light for 5 min at different releasing stages.

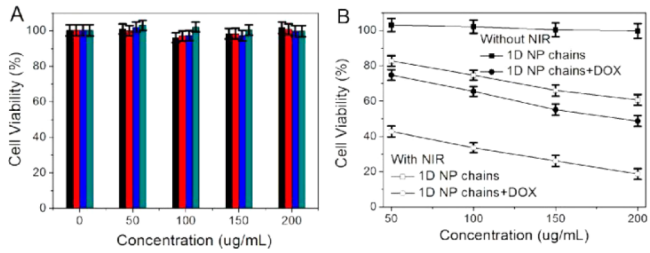

Figure 8. In vitro cytotoxicity of (A) 1D Fe_3O_4@FC NP chains with different chain lengths synthesized in different magnetization assembling time (corresponding to 0, 1, 3, and 12 h in Figure 1A–D) and (B) drug-free and DOX-loaded 1D Fe_3O_4@FC NP chains without and with 5 min exposure to the 1.5 W/cm^2 NIR light, respectively.

average release rate from fifth to eighth hour is determined to be 4.3%/h, which is much higher than the release rate of 1.1%/h obtained without NIR irradiation. After the removal of the NIR irradiation for a few hours, the drug release rate returns to the original slow rate. It only took about 63 h for 95% of the loaded DOX to be released after applying 5 min of NIR irradiation at releasing stages of 0, 5, 30, and 60 h, respectively. Such a significantly enhanced drug release rate with the assistance of short time exposure to NIR light can be attributed to the intensive local heat produced by the efficient photothermal conversion of the graphene-like fluorescent carbon dots embedded in the carbon shell of the 1D NP chains, because the elevated temperature could speed up the Brownian motion of DOX molecules.[62−64] As demonstrated in Figure S10 in the Supporting Information, the gradual increase in temperature from 37 to 42 °C can clearly enhance the DOX release rate, no matter with or without the assistance of NIR irradiation. Figure S11 in the Supporting Information indicates that the 1D Fe_3O_4@FC NP chains possess excellent NIR light photothermal effect. The temperature of 20 mL aqueous dispersion of the 1D NP chains (100 mg/L) in a round glass vial increases by 23 °C from the initial room temperature of 18 °C after 5 min exposure to the NIR irradiation at a power density of 1.5 W/cm^2, whereas the temperature of water (control) only increases by 9.5 °C under the same condition. The NIR-triggerable drug release rate is another advantage of the 1D Fe_3O_4@FC NP chains for applications as multifunctional drug carriers.

To further evaluate the potential of the 1D Fe_3O_4@FC NP chains for multifunctional drug carrier, we elaborately conducted in vitro cytotoxicity of the 1D NP chains against B16F10 cells. Figure 8A shows the in vitro cytotoxicity of the 1D Fe_3O_4@FC NP chains with different chain lengths, after incubated with the B16F10 cells for 24 h in the concentration range of 50−200 μg/mL. It is clear that the 1D Fe_3O_4@FC NP chains are noncytotoxic even at the high concentration of 200 μg/mL and the 1D NP chain length has no effect on the cell viability. These results may result from the noncytotoxic carbon shell that prevents the direct exposure of the magnetic Fe_3O_4 nanocrystals to the cells. Figure 8B compares the in vitro cytotoxic activity of the drug-free and DOX-loaded 1D Fe_3O_4@FC NP chains without and with 1.5 W/cm^2 NIR irradiation for 5 min, respectively. Although the drug-free 1D Fe_3O_4@FC NP chains have no harm to the cells, the introduction of 5 min NIR irradiation to the cells incubated with the drug-free 1D Fe_3O_4@FC NP chains effectively killed the cells. Depending on the concentrations of the 1D NP chains, 20−35% of cells were killed. This result demonstrates that the 1D Fe_3O_4@FC NP chains can be used as an efficient photothermal agent to kill tumor cells under NIR irradiation. Without the assistance of 5 min NIR irradiation, the DOX-loaded 1D Fe_3O_4@FC NP chains could kill about 25−50% cancer cells as the drug carrier concentration increased from 50 to 200 μg/mL, which is understandable because only about 30% of the loaded DOX can be released in 24 h (Figure 7). In contrast, the addition of 5 min NIR irradiation to the DOX-loaded 1D Fe_3O_4@FC NP chains could kill about 60−80% cancer cells at the same concentrations of drug carriers. The significantly enhanced cytotoxicity of the DOX-loaded 1D Fe_3O_4@FC NP chains in combination with 5 min NIR irradiation can be attributed to the synergistic effect of the chemo-/photothermal therapy.

4. CONCLUSIONS

Multifunctional 1D magnetic and fluorescent hybrid NP chains can be synthesized based on the first preparation of the Fe_3O_4@FC NPs with magnetic Fe_3O_4 nanocrystals clustered in the core and fluorescent carbon dots embedded in the amorphous carbon shell, followed by the assembly of these NPs under an external magnetic field. The surface hydroxyl/carboxyl groups on the carbon shell of the NPs are important to link the NPs stably through the hydrogen bonding and other weak interactions. The lengths of 1D NP chains can be controlled by tuning the induction time of external magnetic field. The resulted 1D Fe_3O_4@FC NP chains not only exhibit strong λ_{ex}-dependent and up-converted fluorescence with excellent photostability, but also have weak ferromagnetism property and high magnetization saturation at room temperature. The newly developed 1D Fe_3O_4@FC NP chains can overcome cellular barriers to enter into the intracellular region and light up the cells. The assembled 1D NP chains also demonstrate much higher MRI contrast than the corresponding building block NPs. While the porous carbon shell of the 1D NP chains can provide high loading capacity for DOX molecules, the fluorescent carbon dots embedded in the carbon shell can provide efficient photothermal conversion ability to enhance the drug release rate with the assistance of NIR light. The 1D Fe_3O_4@FC NP chains are noncytotoxic, but can carry and release DOX drug molecules effectively to kill the B16F10 cells. The combination of the DOX-loaded 1D Fe_3O_4@FC NP chains with 5 min NIR irradiation can dramatically improve the therapeutic efficacy because of the synergistic effect of the chemo-/photothermal therapy.

■ ASSOCIATED CONTENT

Supporting Information

Figures S1−S11. This material is available free of charge via the Internet at http://pubs.acs.org.

■ AUTHOR INFORMATION

Corresponding Author

*E-mail: shuiqin.zhou@csi.cuny.edu. Tel.: +1 718 982 3897. Fax: +1 718 982 3910.

Notes

The authors declare no competing financial interest.

■ ACKNOWLEDGMENTS

We gratefully acknowledge the financial support from the PSC−CUNY Research Award (66076-0044) and American Diabetes Association (Basic Science Award 1-12-BS-243).A portion of this research was conducted at the Center for Nanophase Materials Sciences, which is sponsored at Oak Ridge National Laboratory by the Scientific User Facilities Division, Office of Basic Energy Sciences, U.S. Department of Energy.

■ REFERENCES

(1) Qian, F.; Gradečak, S.; Li, Y.; Wen, C.; Lieber, C. M. Core/Multishell Nanowire Heterostructures as Multicolor, High-efficiency Light-Emitting Diodes. *Nano Lett.* **2005**, *5*, 2287−2291.

(2) Koenig, A.; Hébraud, P.; Gosse, C.; Dreyfus, R.; Baudry, J.; Bertrand, E.; Bibette, J. Magnetic Force Probe for Nanoscale Biomolecules. *Phys. Rev. Lett.* **2005**, *95*, 128301−128304.

(3) Shalek, A. K.; Robinson, J. T.; Karp, E. S.; Lee, J. S.; Ahn, D. R.; Yoon, M. H.; Sutton, A.; Jorgolli, M.; Gertner, R. S.; Gujral, T. S.; MacBeath, G.; Yang, E. G.; Park, H. Vertical Silicon Nanowires as a Universal Platform for Delivering Biomolecules into Living Cells. *Proc. Natl. Acad. Sci. U.S.A.* **2010**, *107*, 1870−1875.

(4) Cui, Y.; Wei, Q.; Park, H.; Lieber, C. M. Nanowire Nanosensors for Highly Sensitive and Selective Detection of Biological and Chemical Species. *Science* **2001**, *293*, 1289−1292.

(5) Kim, W.; Ng, J. K.; Kunitake, M. E.; Conklin, B. R.; Yang, P. Interfacing Silicon Nanowires with Mammalian Cells. *J. Am. Chem. Soc.* **2007**, *129*, 7228−7229.

(6) Patolsky, F.; Zheng, G.; Lieber, C. M. Fabrication of Silicon Nanowire Devices for Ultrasensitive, Label-free, Real-Time Detection of Biological and Chemical Species. *Nat. Protoc.* **2006**, *1*, 1711−1724.

(7) Patolsky, F.; Zheng, G.; Lieber, C. M. Nanowire-Based Biosensors. *Anal. Chem.* **2006**, *78*, 4260−4269.

(8) Patolsky, F.; Zheng, G.; Lieber, C. M. Nanowire Sensors for Medicine and The Life Sciences. *Nanomedicine* **2006**, *1*, 51−65.

(9) Uskoković, V.; Lee, K.; Lee, P. P.; Fischer, K. E.; Desai, T. A. Shape Effect in The Design of Nanowire-Coated Microparticles as Transepithelial Drug Delivery Devices. *ACS Nano* **2012**, *6*, 7832−7841.

(10) Park, J. H.; von Maltzahn, G.; Zhang, L.; Schwartz, M. P.; Ruoslahti, E.; Bhatia, S. N. Sailor, M. J. Magnetic Iron Oxide Nanoworms for Tumor Targeting and Imaging. *Adv. Mater.* **2008**, *20*, 1630−1635.

(11) Hultgren, A.; Tanase, M.; Felton, E. J.; Bhadriraju, K.; Salem, A. K.; Chen, C. S.; Reich, D. H. Optimization of Yield in Magnetic Cell Separations Using Nickel Nanowires of Different Lengths. *Biotechnol. Prog.* **2005**, *21*, 509−515.

(12) Hultgren, A.; Tanase, M.; Chen, C. S.; Meyer, G. J.; Reich, D. H. Cell Manipulation Using Magnetic Nanowires. *J. Appl. Phys.* **2003**, *93*, 7554−7556.

(13) Tanase, M.; Felton, E. J.; Gray, D. S.; Hultgren, A.; Chen, C. S.; Reich, D. H. Assembly of Multicellular Constructs and Microarrays of Cells Using Magnetic Nanowires. *Lab Chip* **2005**, *5*, 598−605.

(14) Zhang, L.; Petit, T.; Peyer, K. E.; Nelson, B. J. Targeted Cargo Delivery Using a Rotating Nickel Nanowire. *Nanomedicine* **2012**, *8*, 1074−1080.

(15) Gao, N.; Wang, H.; Yang, E. H. An Experimental Study on Ferromagnetic Nickel Nanowires Functionalized with Antibodies for Cell Separation. *Nanotechnology* **2010**, *21*, 105107−105114.

(16) Lin, Y. C.; Kramer, C. M.; Chen, C. S.; Reich, D. H. Probing Cellular Traction Forces with Magnetic Nanowires and Microfabricated Force Sensor Arrays. *Nanotechnology* **2012**, *23*, 075101−075108.

(17) Goubault, C.; Jop, P.; Fermigier, M.; Baudry, J.; Bertrand, E.; Bibette, J. Flexible Magnetic Filaments as Micromechanical Sensors. *Phys. Rev. Lett.* **2003**, *91*, 2608021−2608024.

(18) Yue, Z.; Wei, W.; You, Z.; Yang, Q.; Yue, H.; Su, Z.; Ma, G. Iron Oxide Nanotubes for Magnetically Guided Delivery and pH-Activated Release of Insoluble Anticancer Drugs. *Adv. Funct. Mater.* **2011**, *21*, 3446−3453.

(19) Johansson, F.; Jonsson, M.; Alm, K.; Kanje, M. Cell Guidance by Magnetic Nanowires. *Exp. Cell Res.* **2010**, *316*, 688−694.

(20) Song, M. M.; Song, W. J.; Bi, H.; Wang, J.; Wu, W. L.; Sun, J.; Yu, M. Cytotoxicity and Cellular Uptake of Iron Nanowires. *Biomaterials* **2010**, *31*, 1509−1517.

(21) Fakhrullin, R. F.; Bikmullin, A. G.; Nurgaliev, D. K. Magnetically Responsive Calcium Carbonate Microcrystals. *ACS Appl. Mater. Interfaces* **2009**, *1*, 1847−1851.

(22) Jia, J.; Yu, J. C.; Wang, Y. J.; Chan, K. M. Magnetic Nanochains of $FeNi_3$ Prepared by A Template-Free Microwave-Hydrothermal Method. *ACS Appl. Mater. Interfaces* **2010**, *2*, 2579−2584.

(23) Lee, C. M.; Jeong, H. J.; Lim, S. T.; Sohn, M. H.; Kim, D. W. Synthesis of Iron Oxide Nanoparticles with Control Over Shape Using Imidazolium-Based Ionic Liquids. *ACS Appl. Mater. Interfaces* **2010**, *2*, 756−759.

(24) Choi, J. H.; Nguyen, F. T.; Barone, P. W.; Heller, D. A.; Moll, A. E.; Patel, D.; Boppart, S. A.; Strano, M. S. Multimodal Biomedical Imaging with Asymmetric Single-Walled Carbon Nanotube/Iron Oxide Nanoparticle Complexes. *Nano Lett.* **2007**, *7*, 861−867.

(25) Correa-Duarte, M. A.; Grzelczak, M.; Salgueiriño-Maceira, V.; Giersig, M.; Liz-Marzan, L. M.; Farle, M.; Sierazdki, K.; Diaz, R. Alignment of Carbon Nanotubes Under Low Magnetic Fields Through Attachment of Magnetic Nanoparticles. *J. Phys. Chem. B* **2005**, *109*, 19060−19063.

(26) Fresnais, J.; Berret, J. F.; Frka-Petesic, B.; Sandre, O.; Perzynski, R. Electrostatic Co-Assembly of Iron Oxide Nanoparticles and Polymers: Towards The Generation of Highly Persistent Superparamagnetic Nanorods. *Adv. Mater.* **2008**, *20*, 3877−3881.

(27) Fresnais, J.; Ishow, E.; Sandre, O.; Berret, J. F. Electrostatic Co-Assembly of Magnetic Nanoparticles and Fluorescent Nanospheres: A Versatile Approach Towards Bimodal Nanorods. *Small* **2009**, *5*, 2533−2536.

(28) Yan, M.; Fresnais, J.; Sekar, S.; Chapel, J. P.; Berret, J. F. Magnetic Nanowires Generated via The Waterborne Desalting Transition Pathway. *ACS Appl. Mater. Interfaces* **2011**, *3*, 1049−1054.

(29) Safi, M.; Yan, M.; Guedeau-Boudeville, M.; Conjeaud, H.; Garnier-Thibaud, V.; Boggetto, N.; Baeza-Squiban, A.; Niedergang, F.; Averbeck, D.; Berret, J. F. Interactions Between Magnetic Nanowires and Living Cells: Uptake, Toxicity, and Degradation. *ACS Nano* **2011**, *5*, 5354−5364.

(30) Nakata, K.; Hu, Y.; Uzun, O.; Bakr, O.; Stellacci, F. Chains of Superparamagnetic Nanoparticles. *Adv. Mater.* **2008**, *20*, 4294−4299.

(31) Byrne, S. J.; Corr, S. A.; Gun'ko, Y. K.; Kelly, J. M.; Brougham, D. F.; Ghoshb, S. Magnetic Nanoparticle Assemblies on Denatured DNA Show Unusual Magnetic Relaxivity and Potential Applications for MRI. *Chem. Commun.* **2004**, 2560−2561.

(32) Corr, S. A.; Byrne, S. J.; Tekoriute, R.; Meledandri, C. J.; Brougham, D. F.; Lynch, M.; Kerskens, C.; O'Dwyer, L.; Gun'ko, Y. K. Linear Assemblies of Magnetic Nanoparticles as MRI Contrast Agents. *J. Am. Chem. Soc.* **2008**, *130*, 4214−4215.

(33) Jaganathan, H.; Hugar, D. L.; Ivanisevic, A. Examining MRI Contrast in Three-Dimensional Cell Culture Phantoms With DNA-

Templated Nanoparticle Chains. *ACS Appl. Mater. Interfaces* **2011**, *3*, 1282−1288.
(34) Jurez, J.; Cambn, A.; Topete, A.; Taboada, P.; Mosquera, V. One-Dimensional Magnetic Nanowires Obtained by Protein Fibril Biotemplating. *Chem.—Eur. J.* **2011**, *17*, 7366−7373.
(35) Park, J. H.; von Maltzahn, G.; Zhang, L.; Derfus, A. M.; Simberg, D.; Harris, T. J.; Ruoslahti, E.; Bhatia, S. N.; Sailor, M. J. Systematic Surface Engineering of Magnetic Nanoworms for In Vivo Tumor Targeting. *Small* **2009**, *5*, 694−700.
(36) Sheparovych, R.; Sahoo, Y.; Motornov, M.; Wang, S.; Luo, H.; Prasad, P. N.; Sokolov, I.; Minko, S. Polyelectrolyte Stabilized Nanowires from Fe_3O_4 Nanoparticles via Magnetic Field Induced Self-Assembly. *Chem. Mater.* **2006**, *18*, 591−593.
(37) Wang, C.; Chen, J.; Talavage, T.; Irudayaraj, J. Gold Nanorod/Fe_3O_4 Nanoparticle "Nano-Pearl-Necklaces" for Simultaneous Targeting, Dual-Mode Imaging, and Photothermal Ablation of Cancer Cells. *Angew. Chem., Int. Ed.* **2009**, *48*, 2759−2763.
(38) Motornov, M.; Malynych, S.; Pippalla, D.; Zdyrko, B.; Royter, H.; Roiter, Y.; Kahabka, M.; Tokarev, A.; Tokarev, I.; Zhulina, E.; Kornev, K.; Luzinov, I.; Minko, S. Field-Directed Self-Assembly with Locking Nanoparticles. *Nano Lett.* **2012**, *12*, 3814−3820.
(39) Peiris, P. M.; Bauer, L.; Toy, R.; Tran, E.; Pansky, J.; Doolittle, E.; Schmidt, E.; Hayden, E.; Mayer, A.; Keri, R. A.; Griswold, M. A.; Karathanasis, E. Enhanced Delivery of Chemotherapy to Tumors Using A Multicomponent Nanochain with Radio-Frequency-Tunable Drug Release. *ACS Nano* **2012**, *6*, 4157−4168.
(40) Peiris, P. M.; Toy, R.; Abramowski, A.; Vicente, P.; Tucci, S.; Bauer, L.; Mayer, A.; Tam, M.; Doolittle, E.; Pansky, J.; Tran, E.; Lin, D.; Schiemann, W. P.; Ghaghada, K. B.; Griswold, M. A.; Karathanasis, E. Treatment of Cancer Micrometastasis Using A Multicomponent Chain-Like Nanoparticle. *J. Controlled Release* **2014**, *173*, 51−58.
(41) Serantes, D.; Simeonidis, K.; Angelakeris, M.; Chubykalo-Fesenko, O.; Marciello, M.; del Puerto Morales, M.; Baldomir, D.; Martinez-Boubeta, C. Multiplying Magnetic Hyperthermia Response by Nanoparticle Assembling. *J. Phys. Chem. C* **2014**, *118*, 5927−5934.
(42) Wang, H.; Chen, Q.; Sun, L.; Qi, H.; Yang, X.; Zhou, S.; Xiong, J. Magnetic-Field-Induced Formation of One-Dimensional Magnetite Nanochains. *Langmuir* **2009**, *25*, 7135−7139.
(43) Zhang, Z.; Duan, H.; Li, S.; Lin, Y. Assembly of Magnetic Nanospheres into One-Dimensional Nanostructured Carbon Hybrid Materials. *Langmuir* **2010**, *26*, 6676−6680.
(44) Wang, H.; Sheng, J.; Li, Y.; Wei, Z.; Cao, G.; Gai, Z.; Hong, K.; Banerjee, P.; Zhou, S. Magnetic Iron Oxide−Fluorescent Carbon Dots Integrated Nanoparticles for Dual-Modal Imaging, Near-Infrared Light-Responsive Drug Carrier and Photothermal Therapy. *Biomater. Sci.* **2014**, *2*, 915−923.
(45) Duffy, P.; Magno, L.; Yadav, R.; Roberts, S. K.; Ward, A. D.; Botchway, S. W.; Colavita, P. E.; Quinn, S. J. Incandescent Porous Carbon Microspheres to Light Up Cells: Solution Phenomena and Cellular Uptake. *J. Mater. Chem.* **2012**, *22*, 432−439.
(46) Socrates, G. *Infrared and Raman characteristic group frequencies: Tables and Charts*, 3rd ed; John Wiley& Sons Ltd: Chichester, 2001.
(47) Coates, J. Interpretation of Infrared Spectra, A Practical Approach. In *Encyclopedia of Analytical Chemistry*; Meyers, R. A., Ed.; John Wiley & Sons: Chichester, U.K., 2000; pp 10815−10837.
(48) Tian, L.; Ghosh, D.; Chen, W.; Pradhan, S.; Chang, X.; Chen, S. Nanosized Carbon Particles from Natural Gas Soot. *Chem. Mater.* **2009**, *21*, 2803−2809.
(49) Yu, S. J.; Kang, M. W.; Chang, H. C.; Chen, K. M.; Yu, Y. C. Bright Fluorescent Nanodiamonds: No Photobleaching and Low Cytotoxicity. *J. Am. Chem. Soc.* **2005**, *127*, 17604−17605.
(50) Chang, Y. R.; Lee, H. Y.; Chen, K.; Chang, C. C.; Tsai, D. S.; Fu, C. C.; Lim, T. S.; Tzeng, Y. K.; Fang, C. Y.; Han, C. C.; Chang, H.; Fan, W. Mass Production and Dynamic Imaging of Fluorescent Nanodiamonds. *Nat. Nanotechnol.* **2008**, *3*, 284−288.
(51) Wang, F.; Pang, S. P.; Wang, L.; Li, Q.; Kreiter, M.; Liu, C. Y. One-Step Synthesis of Highly Luminescent Carbon Dots in Noncoordinating Solvents. *Chem. Mater.* **2010**, *22*, 4528−4530.
(52) Cao, L.; Wang, X.; Meziani, M.; Lu, F.; Wang, H.; Luo, P.; Lin, Y.; Harruff, B.; Veca, L.; Murray, D.; Xie, S.; Sun, Y. Carbon Dots for Multiphoton Bioimaging. *J. Am. Chem. Soc.* **2007**, *129*, 11318−11319.
(53) Fang, Y.; Guo, S.; Li, D.; Zhu, C.; Ren, W.; Dong, S.; Wang, E. Easy Synthesis and Imaging Applications of Cross-Linked Green Fluorescent Hollow Carbon Nanoparticles. *ACS Nano* **2012**, *6*, 400−409.
(54) Wu, X.; Liu, H.; Liu, J.; Haley, K. N.; Treadway, J. A.; Larson, J. P.; Ge, N.; Peale, F.; Bruchez, M. P. Immunofluorescent Labeling of Cancer Marker Her2 and Other Cellular Targets with Semiconductor Quantum Dots. *Nat. Biotechnol.* **2003**, *21*, 41−46.
(55) Zhang, F.; Wang, C. Fabrication of One-Dimensional Iron Oxide/Silica Nanostructures with High Magnetic Sensitivity by Dipole-Directed Self-Assembly. *J. Phys. Chem. C* **2008**, *112*, 15151−15156.
(56) Saville, S. L.; Woodward, R. C.; House, M. J.; Tokarev, A.; Hammers, J.; Qi, B.; Shaw, J.; Saunders, M.; Varsani, R. R.; St Pierre, T. G.; Mefford, O. T. The Effect of Magnetically Induced Linear Aggregates on Proton Transverse Relaxation Rates of Aqueous Suspensions of Polymer Coated Magnetic Nanoparticles. *Nanoscale* **2013**, *5*, 2152−2163.
(57) Nasongkla, N.; Bey, E.; Ren, J.; Ai, H.; Khemtong, C.; Guthi, J. S.; Chin, S.; Sherry, A. D.; Boothman, D. A.; Gao, J. Multifunctional Polymeric Micelles as Cancer-Targeted, MRI-Ultrasensitive Drug Delivery Systems. *Nano Lett.* **2006**, *6*, 2427−2430.
(58) Bianco, A.; Kostarelos, K.; Partidos, C. D.; Prato, M. Biomedical Applications of Functionalised Carbon Nanotubes. *Chem. Commun.* **2005**, *5*, 571−577.
(59) Kostarelos, K.; Lacerda, L.; Pastorin, G.; Wu, W.; Wieckowski, S.; Luangsivilay, J.; Godefroy, S.; Pantarotto, D.; Briand, J.; Muller, S.; Prato, M.; Bianco, A. Cellular Uptake of Functionalized Carbon Nanotubes Is Independent of Functional Group and Cell Type. *Nat. Nanotechnol.* **2007**, *2*, 108−113.
(60) Pantarotto, D.; Singh, R.; Mccarthy, D.; Erhardt, M.; Briand, J. P.; Prato, M.; Kostarelos, K.; Bianco, A. Functionalized Carbon Nanotubes for Plasmid DNA Gene Delivery. *Angew. Chem., Int. Ed.* **2004**, *43*, 5242−5246.
(61) Hughes, D. L.; Reamer, R. A. The Effect of Acid Strength on The Mitsunobu Esterification Reaction: Carboxyl vs Hydroxyl Reactivity. *J. Org. Chem.* **1996**, *61*, 2967−71.
(62) Yang, K.; Zhang, S.; Zhang, G.; Sun, X.; Lee, S.; Liu, Z. Graphene In Mice: Ultrahigh In Vivo Tumor Uptake and Efficient Photothermal Therapy. *Nano Lett.* **2010**, *10*, 3318−3323.
(63) Wang, H.; Shen, J.; Cao, G.; Gai, Z.; Hong, K. L.; Debata, P. R.; Banerjee, P.; Zhou, S. Multifunctional PEG Encapsulated Fe_3O_4@Silver Hybrid Nanoparticles: Antibacterial Activity, Cell Imaging and Combined Photothermo/Chemo-Therapy. *J. Mater. Chem. B* **2013**, *1*, 6225−6234.
(64) Wang, H.; Ke, F.; Mararenko, A.; Wei, Z.; Banerjee, P.; Zhou, S. Responsive Polymer-fluorescent Carbon Nanoparticle Hybrid Nanogels for Optical Temperature Sensing, Near-infrared Light-responsive Drug Release, and Tumor Cell Imaging. *Nanoscale* **2014**, *6*, 7443−7452.